Adipose-Derived Stromal Cell Secreted Factors Induce the Elastogenesis Cascade within 3D Aortic Medial Layer Equivalents

Aneesh K Ramaswamy[1], Rachel E Sides[1], Eoghan M Cunnane[1,2], Katherine L Lorentz[1], Leila M Reines[1], David A Vorp[1,3,4,5,6], Justin S Weinbaum[1,3,7]

1: Department of Bioengineering, University of Pittsburgh, Pittsburgh, PA, United States of America
2: Tissue Engineering Research Group, Department of Anatomy, Royal College of Surgeons in Ireland, Dublin, Ireland
3: McGowan Institute for Regenerative Medicine, University of Pittsburgh, Pittsburgh, PA, United States of America
4: Department of Surgery, University of Pittsburgh, Pittsburgh, PA, United States of America
5: Department of Cardiothoracic Surgery, University of Pittsburgh, Pittsburgh, PA, United States of America
6: Department of Chemical and Petroleum Engineering, University of Pittsburgh, Pittsburgh, PA, United States of America
7: Department of Pathology, University of Pittsburgh, Pittsburgh, PA, United States of America

Corresponding Author:
Justin Weinbaum
Department of Bioengineering
University of Pittsburgh
Center for Bioengineering, Suite 300
300 Technology Drive
Pittsburgh, PA 15261
(412) 624-9242
juw51@pitt.edu

Abstract:

Objective: Elastogenesis within the medial layer of the aortic wall involves a cascade of events orchestrated primarily by smooth muscle cells, including transcription of elastin and a cadre of elastin chaperone matricellular proteins, deposition and cross-linking of tropoelastin coacervates, and maturation of extracellular matrix fiber structures to form mechanically competent vascular tissue. Elastic fiber disruption is associated with aortic aneurysm; in aneurysmal disease a thin and weakened wall leads to a high risk of rupture if left untreated, and non-surgical treatments for small aortic aneurysms are currently limited. This study analyzed the effect of adipose-derived stromal cell secreted factors on each step of the smooth muscle cell elastogenesis cascade within a three-dimensional fibrin gel culture platform.

Approach and results: We demonstrate that adipose-derived stromal cell secreted factors induce an increase in smooth muscle cell transcription of tropoelastin, fibrillin-1, and chaperone proteins fibulin-5, lysyl oxidase, and lysyl oxidase-like 1, formation of extracellular elastic fibers, insoluble elastin and collagen protein fractions in dynamically-active 30-day constructs, and a mechanically competent matrix after 30 days in culture.

Conclusion: Our results reveal a potential avenue for an elastin-targeted small aortic aneurysm therapeutic, acting as a supplement to the currently employed passive monitoring strategy. Additionally, the elastogenesis analysis workflow explored here could guide future mechanistic studies of elastin formation, which in turn could lead to new non-surgical treatment strategies.

Highlights:

1. Stromal cells stimulate smooth muscle cells (SMC) using paracrine signals.
2. Stimulated SMC make RNA for both elastin and associated proteins.
3. After protein synthesis, new elastic fibers form that contain insoluble elastin.
4. Stromal cell products could promote elastin production in vivo.

Key words: aorta, aneurysm, elastin, vasculature, vascular regeneration

1 Introduction

Aortic aneurysms (AAs) are balloon-like enlargements of the aorta that pose a life-threatening risk of rupture. AAs are most prominent in both aging populations (primarily smokers) and pediatric or young adult patients with connective tissue genetic disorders [1]. Approximately 5 million Americans over the age of 50 are living with abdominal or thoracic AA [2,3], with over 200,000 new AAs diagnosed annually [4]. Actively dilating AAs, if left untreated, can weaken and ultimately rupture or dissect, with over 15,000 annual AA ruptures/dissections [5,6] and an 80–90% AA mortality rate upon rupture representing the 15th leading cause of death in the United States [[7], [8], [9]].

One feature of AA dilation is the degradation of elastin, the extracellular matrix (ECM) protein within the aortic wall responsible for recoil forces during diastole. Smooth muscle cells (SMCs) form mature elastin during early childhood stages of human development, and the expression of tropoelastin (elastin core protein) and elastin organizational matricellular proteins (such as specific members of the fibrillin, fibulin, lysyl oxidase, and latent transforming growth factor β binding protein, or LTBP, families) are then downregulated during adulthood [10, 11]. Mechanical wall stress [12, 13, 14], inflammatory response and proteolytic degradation [15, 16, 17], and exogenous circulating growth factors (primarily activating the TGF-β pathway) [18] have been shown to disrupt local AA SMCs and elastic fibers [19], leading to increased risk of rupture.

Currently, endovascular aortic repair is the standard intervention for abdominal AA, with aortic diameter measurements determining the threshold for surgical intervention. Adults are diagnosed with AA once the aortic diameter exceeds ~1.5-times its normal

value, and surgical intervention of repair is generally recommended after the AA exceeds a “critical diameter” of ~5.5 cm and 1 cm/year growth rate [7,20]. Standard non-surgical options for patients with small abdominal AA (classified as an AA with a diameter above the aneurysmal classification threshold but below the “critical” threshold) are limited to semi-annual ultrasound or computerized tomography imaging surveillance, with current pharmacological agents providing minimal evidence of AA-targeted effects [21,22].

However, 23.4% of sub-critical adult abdominal AAs ranging between 4.1 and 5.5 cm rupture [23], underscoring the need for a targeted, non-surgical therapeutic option for dilating AAs. A targeted regenerative treatment, wherein functional elastic fibers are restored, could offer a non-surgical therapeutic option for adults with small abdominal AA, and a maintenance therapy for children with connective tissue disorders that affect the vasculature. Pediatric patients with “rapid aortic expansion” of AA (exceeding 0.5 cm/year rate) typically undergo surgical intervention, often with several repeated surgeries and broad-targeted therapies (beta blockers, angiotensin-converting enzyme inhibitors) prescribed [22, [24], [25], [26]]. An elastin-targeted therapeutic available for patients with small sub-critical AA is a critical need as a supplement to standard surveillanc protocols.

Previous work by our lab has shown that periadventitial adipose-derived stromal cell (ASC) delivery to a growing elastase-induced mouse abdominal AA halts aneurysmal growth, prevents further elastin degradation, and possibly stimulates new elastin synthesis, as evidenced by maintenance of elastic lamellae [27]. It is hypothesized that ASCs help maintain existing elastic fibers by modulating SMC phenotype to repress

immune inflammatory response in local AA tissue [28], suppress elastin breakdown [29], or stimulate new elastin deposition [30]. While it was initially theorized that these ASC subpopulations differentiate into functional vascular cells [31], subsequent studies have suggested that ASC secreted factors (ASC-SF) act in a paracrine manner on neighboring vascular host SMC and endothelial cells, specifically pointing to the importance of urokinase-type plasminogen activator [32] and monocyte chemoattractant protein-1 [33] in remodeling. ASC-SF are rich in pro-angiogenic [34] and pro-inflammatory growth factors [35] (vascular endothelial growth factor, hepatocyte growth factor, interleukin-1β, interleukin-6, interleukin-8, tumor necrosis factor-α) which play important roles in SMC ECM deposition [29,36].

While multiple mechanisms can potentially explain the efficacy of ASC in the mouse model [27], the present study tested whether paracrine signaling, through ASC-SF, could induce deposition of elastin by healthy adult aortic SMCs in three-dimensional (3D) in vitro culture. The elastogenesis cascade requires a cadre of ECM accessory proteins for proper elastin processing and assembly (Fig. 1), and these proteins must be monitored in a context that combines cellular biology with regenerative tissue engineering. Our study utilized a versatile, fibrin-based 3D SMC culture platform [37,38] to analyze ASC-SF induced elastin deposition at four different points of interest on the elastogenesis cascade: elastin organizational protein transcription (generating tropoelastin, fibulin-4, and fibulin-5 coacervates/globules) [[39], [40], [41]], elastic fiber organization (through LTBP-4, fibulin-4, and fibulin-5 mediated deposition onto fibrillin-1 microfibrils) [[42], [43], [44], [45]], cross-linked elastin chemical maturity (mediated by lysyl oxidase or LOX, and lysyl oxidase-like 1 or LOXL-1) [46,47], and mechanical

functionality. In addition, post-translational modification and mechanical function of the counterpart vascular ECM protein collagen were also studied.

2 Results

As a brief overview of the model and the terminology to be used, human aortic SMCs (ATCC) were cultured within 3D fibrin gel constructs, either as “discs” on multi-well tissue culture plastic or “strands” on FlexCell Linear TissueTrain flexible culture plates. Strands were cultured in two conditions: “constrained”, cultured without any external mechanical stimulation but having cell-induced static uniaxial tension; and “dynamic”, with constructs subjected to 10% displacement at 1 Hz mechanical loading conditions. Exogenous media treatments were refreshed every 48–72 h, and elastogenesis cascade analysis was performed after 20 days and 30 days of culture. Control group treatments include “No Treatment” (NT, standard SMC growth media) and “Non-Conditioned Media” (NCM, a 1:1 combination of SMC and fresh ASC growth media). Note that to limit the number of experimental samples to be run (and expense of the TissueTrain plates) the NCM control was only run for discs. Experimental group treatment was “Adipose Stromal Cell Secreted Factors” (ASC-SF, a 1:1 combination of SMC growth media and ASC conditioned media), intended to simulate previously observed pro-elastogenic paracrine effects of ASCs on aortic SMCs [32].

2.1 ASC-SF increase expression of the SMC phenotypic marker myosin heavy chain.

After 30 days of culture, qPCR analysis of discs (Figure 2A) revealed a transcriptional increase in SMC differentiation marker myosin heavy chain after ASC-SF stimulation (3.916 ± 1.952) when compared to both NT control (1 ± 0.0003) and NCM (0.8443 ± 0.6187). No difference was seen in transcription of α smooth muscle actin after ASC-SF stimulation (0.5731 ± 0.2137) when compared to both NT control

(1 ± 0.1319) and NCM (0.4924 ± 0.2644); likewise, no difference was seen in transcription of calponin after ASC-SF stimulation (1.303 ± 0.4857) when compared to both NT control (1 ± 0.2543) and NCM (0.9533 ± 0.2896).

2.2 ASC-SF induce SMC transcription of tropoelastin and elastin chaperone proteins

After 30 days of culture, qPCR analysis of discs revealed that ASC-SF (4.94 ± 0.71-fold increase vs NT control, $p < 0.0001$) induced a significant increase in SMC tropoelastin (Fig. 2B). NCM also increased tropoelastin expression (3.09 ± 0.29-fold increase vs NT control, $p = 0.001$). ASC-SF also uniquely increased SMC transcription of microfibril protein fibrillin-1 (4.22 ± 1.10-fold increase, $p = 0.00014$), elastin organizational protein fibulin-5 (5.42 ± 0.53-fold increase, $p < 0.0001$), and cross-linking proteins LOX (2.31 ± 0.44-fold increase, $p = 0.00046$) and LOXL-1 (2.22 ± 0.53-fold increase, $p = 0.0052$). Expression of LTBP-4, responsible for elastin coacervate globule deposition onto fibrillin-1 microfibrils, was significantly downregulated with both ASC-SF stimulation (0.98 ± 0.02-fold decrease versus NT control, $p < 0.0001$) and NCM (0.99 ± 0.02-fold decrease, $p < 0.0001$). Expression of elastin organizational matricellular protein fibulin-4 was unchanged with ASC-SF stimulation. NCM did not induce a significant difference in transcription of fibrillin-1, fibulin-4, fibulin-5, LOX, or LOXL-1, when compared to NT control.

2.3 Elastic fiber deposition increases with ASC-SF treatment

Elastic fibers were clearly distinguishable in ASC-SF stimulated SMC constructs, regardless of geometry, after both 20 days (not shown) and 30 days (Fig. 3A–C). Nuclear count was qualitatively similar between all discs. To expand on the

immunostaining results, discs were also imaged unstained using multiphoton microscopy. In agreement with the results of Fig. 3A–C, multiphoton revealed extensive elastic fibers when discs were cultured with ASC-SF, but not in the NT or NCM controls (Fig. 3D–F). No collagen signal was detected in these samples using second harmonic generation.

2.4 Insoluble elastin increases with ASC-SF treatment after 20 and 30 days of constrained culture regardless of geometry, and after 30 days under dynamic loading of strands

ASC-SF disc stimulation induced a 136% increase versus NT control in insoluble elastin percentage of total protein after 20 days (0.15 ± 0.023% NT control and 0.15 ± 0.03% NCM control, vs 0.37 ± 0.1337% ASC-SF, $p = 0.045$), and a 94% increase after 30 days (0.12 ± 0.04% NT control & 0.098 ± 0.038% NCM control, vs 0.25 ± 0.07% ASC-SF, $p = 0.050$) (Fig. 4A, B).

Insoluble elastin deposition in strands saw a similar 154% increase after 20 days (0.14 ± 0.015% NT control vs 0.36 ± 0.12% ASC-SF, $p = 0.013$) and 124% increase after 30 days (0.13 ± 0.08% NT control vs 0.30 ± 0.076% ASC-SF, $p = 0.0031$) (Fig. 4C). Dynamic SMC constructs, subjected to cyclic uniaxial strain to mimic standard aortic stretching intensity and frequency, produced statistically similar levels of insoluble elastin percentage after 20 days in culture regardless of ASC-SF. After 30 days, however, a 148% increase in elastin percentage was observed (0.29 ± 0.030% NT control vs 0.50 ± 0.069% ASC-SF, $p = 0.016$) (Fig. 4C).

2.5 Collagen fraction increases with ASC-SF treatment after 30 days of disc culture, and after both 20 and 30 days in constrained and dynamic cultured strands

After 20 days of disc culture, ASC-SF stimulation resulted in a statistically similar level of collagen (relative to total protein) when compared to both NT and NCM controls. Extending disc culture to 30 days, however, resulted in a 233% collagen increase with ASC-SF stimulation (0.045% ± 0.028% NT vs 0.15 ± 0.063% ASC-SF, $p = 0.023$). NCM did not result in any detectable collagen after 30 days in culture, despite cellular viability and elastin detection on the same 3D construct set (Fig. 4D, E).

Constrained strands saw ASC-SF induced collagen increases after both 20 days (0.0055 ± 0.0033% NT control vs 0.047 ± 0.0060% ASC-SF, $p = 0.00047$) and 30 days (0.013 ± 0.0032% NT control vs 0.11 ± 0.023% ASC-SF, $p = 0.0026$). Additionally, dynamic cultured strands saw collagen increases after both 20 days (below the detectable threshold for the NT control, vs 0.10 ± 0.026% ASC-SF) and 30 days (NT control below detectable threshold vs 0.19 ± 0.0079% ASC-SF, $p < 0.0001$) (Fig. 4F).

2.6 High-stretch modulus is increased in ASC-SF stimulated strands after 30 days

Cell-free strands displayed an almost linear response to extension (Fig. 5C). The NT strands displayed a more non-linear response and the ASC-SF strands displayed a j-curve type response to extension that is typically exhibited by soft connective tissue, owing to the presence of mechanically functional elastin and collagen. High and low modulus, defined as the slope of the given sample's mechanical response curve within the high stretch range (final third of the curve) and low stretch range (first third of the curve), were then quantified. After 30 days, ASC-SF induced a 151% increase in high

elastic modulus (49.93 ± 8.829 kPa NT control vs 125.2 ± 54.24 kPa ASC-SF, $p = 0.00040$), while low elastic modulus remained statistically unchanged (12.87 ± 7.950 kPa NT control vs 12.90 ± 4.048 kPa ASC-SF) (Fig. 5D). Blank gels displayed a significantly reduced low modulus (5.600 ± 1.335 kPa) and high modulus (8.011 ± 3.634 kPa) in the order of magnitude observed in previous studies with similar cell-free fibrin gels (9–13 kPa) [48]. While all strands were tested to failure, most of the breaks occurred at the nylon tabs versus the middle of the strand, hence ultimate tensile stress is not meaningful enough to report here.

Ninhydrin assays on these tested samples detected a significant increase in insoluble elastin percentage of total protein (0.088 ± 0.028% NT control vs 1.8 ± 0.65% ASC-SF, $p = 0.00074$) when stimulated by ASC-SF. Hydroxyproline assays detected a statistically significant increase in collagen percentage of total protein (0.13 ± 0.077% NT control vs 0.30 ± 0.076% ASC-SF, $p = 0.0031$) when stimulated by ASC-SF.

3 Discussion

The results of this study indicate that ASC-SF treatment induces SMC elastin stimulation within 3D fibrin gel constructs at each level of the elastogenesis cascade: transcription of tropoelastin and other proteins important for elastic fiber assembly/maturation (Fig. 2B), organized elastin fibril formation and networking (Fig. 3), insoluble elastin protein deposition (Fig. 4), and a mechanically-competent extracellular matrix structure incorporating the deposition of collagen within 3D fibrin gel constructs (Fig. 5). The evaluation of elastin at multiple levels in this study is particularly novel compared to other tissue engineering studies where elastin levels are typically only quantified by commercial assay (such as Fastin). The results also compared SMC deposition response when the same fibrin gel construct was plated in two different geometries: “discs” in tissue culture plastic wells versus “strands” on FlexCell Linear TissueTrain flexible silicone wells. Simultaneous evaluation of chemical and mechanical stimulation in the context of tissue engineering adds novelty to this work.

Tropoelastin, the core protein of elastic fibers, sees a nearly 5-fold transcription increase when adult SMCs are stimulated by either ASC-SF or NCM. NCM contains a proprietary formulation developed by the manufacturer (PromoCell) to promote growth of adipose-derived stromal cells – likely this mixture is responsible for the tropoelastin and LTBP-4 transcriptional effects seen with NCM treatment versus SMC media. However, expression of tropoelastin without sufficient support from essential elastin chaperone matricellular proteins results in immature elastic fiber deposition (Fig. 1). In AA, insufficient deposition of elastin chaperone proteins alongside tropoelastin and cross-linked collagen increases aortic stiffness and decreases compliance (caused by

insufficient mature elastin), producing aortic conditions susceptible to rupture [14,49]. In this study, ASC-SF stimulation has shown bioactivity that could address this issue, with significant transcriptional increases in fibulin-5 (which bundles tropoelastin coacervates), LOX (which cross-links tropoelastin via fibulin-4), and LOXL-1 (which cross-links tropoelastin via fibulin-5) (Fig. 2B). Shifts in LOX levels and activity have been noted in other systems, including deficiency of the matricellular protein thrombospondin-2 [50]. Fibrillin-1 is also increased with ASC-SF stimulation, potentially producing more deposition sites for elastin coacervates. While we have not investigated the expression or matrix assembly of microfibril-associated glycoproteins [51] here, they are an interest of the senior author and a target of future study with regards to materials engineering [52]. Notably, ASC-SF also appears to induce a phenotypic switch in adult SMCs (Fig. 2A). While outside the scope of this study, we have initiated collaborations with local experts in SMC biology to investigate this switch further.

While the testing of ASC-SF on matrix production within this study is new, the use of fibrin gels to investigate matrix production is not. Formation of fibrin gels has been of interest to tissue engineers in the context of both cell delivery [53] and tissue repair [54]. Several groups have employed fibrin as a 3D context for embedded cells including mesenchymal stem cells, cardiomyocytes, fibroblasts and smooth muscle cells in order to study tissue remodeling [37], [55], [56], [57], [58], [59], [60], [61], [62], [63], [64], [65], [66], [67], [68], [69], [70], [71]]. The effect of stiffness and dynamic stretch on smooth muscle cell matrix production has also been previously studied both using cell monolayers [72,73] and seeded hydrogels [59], [74], [75], [76]].

In this study, immunostaining and multiphoton microscopy revealed that overall elastic fiber deposition increases with ASC-SF stimulation, potentially mediated by the increased expression of elastic fiber accessory proteins (Fig. 3). New fibers, and intermolecular crosslinking of these fibers, will be ultimately required for a therapy that restores mechanical resilience to the vascular wall. As evidence that elastic fiber cross-linking is occurring, a base hydrolysis method was used to analyze mature elastin content of disc and strand constructs. With the caveat that we did not perform specific testing for lysine crosslinks such as desmosine and isodesmosine (as reviewed in [77]), a clear increase in base-insoluble elastin was observed with ASC-SF treatment at both 20 and 30 days of culture (Fig. 4). While insoluble elastin fraction was increased at both timepoints in discs, collagen fraction only increased after 30 days, indicating either a delay in the transcriptional response for the collagen response or a modulatory effect of the changing ECM on cellular signaling.

Strand constructs displayed key elastin deposition differences between constrained and dynamic cultures. Constrained strands saw increased insoluble elastin fraction after 20 days, while dynamic cultured strands saw the same response only after 30 days. These results suggest that dynamically-active constructs plated on flexible soft substrates, which are more accurate mimics of in vivo aortic conditions, may require an extended ASC-SF therapeutic window to produce chemically mature and mechanically competent elastic fibers in patients with AA. This “delayed” elastogenic effect is of particular interest to bioengineers developing non-surgical therapeutic options tailored for small AA, with 30 days of the current ASC-SF delivery concentration every 48–72 h as the baseline for generating mature elastin from SMCs. We would also contend that

the results of our study have potential applications in a variety of elastin-related diseases (see [78,79] for relevant reviews) beyond AA.

ASC-SF treatment increases the high modulus, but not low modulus, of strands after 30 days of culture compared to the NT and fibrin-only controls (Fig. 5C, D). Elastin, a linearly elastic material, is expected to influence the low-stretch modulus of the gels, as it provides elasticity in the low stretch region of the mechanical response curve to decrease the low modulus of native vessels [[80], [81], [82]]. Mechanical characterization in this study does not reveal a significant difference between the low-stretch modulus of the ASC-SF treated gels relative to the NT group, therefore suggesting that the elastin present in both sets of gels is statistically similar in mechanical function despite the former displaying relatively increased deposition and organization. It should be noted that the strands treated with ASC-SF achieved a comparable but not equivalent maximum tangent modulus to cell-seeded fibrin gels reported by the Billar group (125 kPa in this study vs 221 kPa in Adebayo et al.) [55]. In comparison to other reported studies where dynamic mechanical stimuli and additives such as ascorbic acid and TGF-β were added, our strands exhibited a significantly lower elastic modulus [58,59]. The overall mechanical response of ASC-SF treated gels was similar to the passive mechanical response of the porcine coronary artery [83].

Fig. 5 characterizes the elastic (non-time dependent) mechanical response of the gels; however, elastin also plays an important role in the viscous (time dependent) mechanical response [84]. It is therefore possible that despite displaying statistically similar low-stretch modulus, the ASC-SF treated group could display more physiologically relevant viscous mechanical properties (such as increased creep

resistance) relative to NT controls. Future elastogenesis studies should therefore characterize viscous mechanical properties to further characterize the mechanical functionality of ASC-SF mediated elastin formation relative to NT control. Particular attention should be afforded to creep resistance, which would aid in resisting aneurysm growth over time.

Collagen deposition, mediated by ASC-SF (Fig. 4D), appears to significantly increase the high-stretch modulus of the gels (Fig. 5C, D). ASC-SF treatment also causes the gels to display a stretch-stiffening response that is characteristic of native arterial tissue and attributed to the de-crimping and elongation of collagen fibers [81,85]. Collagen deposition is often defective in AA whereby fibers are not correctly oriented or crimped [86]. The collagen deposited in this study displays evidence of crimping as the mechanical response curves show a clear toe region and stretch-stiffening response. ASC-SF treatment therefore demonstrates the potential to not only trigger the deposition of mechanically competent elastin, but also crimped collagen fibers, both of which would contribute to halting AA growth, reducing rupture risk, and restoring homeostasis.

By coupling elastin matricellular protein transcription with elastic fiber imaging, ECM protein quantification, and mechanical testing, the elastogenesis cascade analysis method outlined in this study illustrates the multiple levels of elastin production by SMCs after ASC-SF therapy. Future work would look to tailor this 3D construct platform to more accurately mimic aneurysmal aorta by seeding SMCs explanted from aneurysmal aortas, altering the stiffness of fibrin constructs, or modulating the stretch parameters of the dynamic culture system. Additionally, a further look into collagen phenotype and the

role of proteoglycans in matrix formation can be studied. Finally, studying the effect of ASC-SF on elastolytic activity [87] will be important for understanding elastin homeostasis generally in the context of disease.

ASCs are known to secrete a variety of factors [35] that could be beneficial in the context of vascular remodeling – a detailed review by our group on the use of these factors in vascular engineering has been published elsewhere [88]. Some of these factors, for example TGF-β [3], HGF, VEGF, IGF, PDGF, and pro-inflammatory factors within the interleukin family [89], could act on host cells to shift them towards a synthetic phenotype. ASCs in a rat model of AAA also result in a damping of elastolysis, as measured by decreased activity of MMP2 and MMP9 [90]. We would hypothesize that it is a synergistic combination of new elastin synthesis (as shown here), decreased elastin degradation, and modulation of the immune system that will lead to regenerative therapy for AAA – such a combination is simply not possible with a single factor.

This study is a first step towards understanding the therapeutic effect of ASC-SF on aortic SMC elastogenesis. It also provides a baseline for ASC-SF delivery concentration when compared to whole-cell therapeutic strategies, with extended release of ASC-SF as a goal for any future elastin-targeted therapeutic approach that utilizes ASC paracrine signaling pathways to benefit SMCs.

4 Materials and Methods

4.1 SMC cell culture conditions.

Human aortic SMCs were purchased from ATCC (ATCC #PCS-100-012, Manassas, Virginia). All cultures were performed at 37˚C and 5% CO2, with growth media (#311K-500, Cell Applications Inc, San Diego, CA) changes every 48-72 hours. Cells used in experimental cultures were between passages 4 and 12.

4.2 Fabrication of 3D SMC-fibrin gel disc and strand constructs.

SMC-seeded fibrin gel constructs [38,57] were formed using 3.7 mg/mL bovine fibrinogen type I (Sigma-Aldrich #8630), 0.21 U/mL bovine thrombin (Sigma-Aldrich #T7513), and 5 × 105 SMCs/mL. 'Disc' 200 μL fibrin gel constructs (Fig. 6A) were seeded within heat- stamped circular molds made using 7.94 mm (5/16″) diameter cork borers onto tissue-culture treated plastic. "Strand" 600 μL fibrin gel constructs (Fig. 6B) were formed between nylon anchors of FlexCell Linear TissueTrain untreated plates (FlexCell Int'l Corp #T-5001U), with "constrained" constructs cultured without external mechanical stimuli. Note that the discs are cultured on top of stiff tissue culture plastic while strands are cultured on top of a flexible silicone membrane. "Dynamic" strands were subjected to a 10% stretch at 1 Hz cyclic uniaxial mechanical loading using a FlexCell FX-4000 strain unit, to mimic standard aortic cardiovascular conditions [76]. Epsilon-amino caproic acid (ACA) (Sigma-Aldrich #07260), a lysine-mimicking fibrinolysis inhibitor, was added at 12 mM to all construct culture media to inhibit cell-driven degradation of the fibrin gel constructs. Treatment changes were made every 48–72 h, beginning 24 h after initial gel polymerization and continuing through harvest at 20- or 30-days post-fabrication.

4.3 ASC culture conditions and conditioned media collection.

ASCs were obtained from deidentified waste human adipose tissue collected during body sculpting surgeries of non-smoking, non-diabetic patients under 45 years old at UPMC Presbyterian Hospital (Fig. 6C). 100 mL of human adipose tissue was mechanically minced and digested in collagenase (1 mg/mL) and bovine serum albumin (35 mg/mL) (protease free heat shock, Equitech-Bio Inc. #BAH65), followed by filtration and heating (1 h in a 37 °C shaker bath) [91,92]. After secondary filtration (0.5 mm gauze, ThermoFisher Scientific #22-415-469) to remove large particles, samples were centrifuged at 1000 rpm and 4 °C for 10 min, with pellets resuspended in 10 mL of ACK Lysing Buffer (ThermoFisher Scientific #A10492-01). The suspension was passed through a sieve (500 µm, pluriSelect #43-50500-01) and centrifuged again under the same conditions. This ASC pellet was resuspended in “ASC culture media”, consisting of 33% Dulbecco's Modified Eagles Medium (High Glucose, Gibco #12100046), 33% DMEM/F12 Medium (HEPES, Gibco #12400024), 7.5% fetal bovine serum (FBS, Premium Select Atlanta Biologics #S11550), 0.75% fungizone (Lonza BioWhittaker Antibiotics #BW17836E), 0.75% penicillin streptomycin (10,000 U/mL, ThermoFisher Scientific #15140122), 0.075 µM Dexamethasone (Sigma-Aldrich #D4902), and 25% Preadipocyte Growth Medium (PromoCell #C-39425). ASC conditioned media was collected every 24–72 h between passage 0 and 1 while cells progressed from 40 to 70% confluence, and immediately frozen at −80 °C.

4.4 Flow cytometry ASC cell sorting.

After 1 week of culture and 1 passage, 2.5 million ASCs were suspended in 1 mL phosphate buffered saline (pH 7.4, Gibco #10010023) and 2% FBS (Premium Select,

Atlanta Biologics # S11550). Each ASC suspension was stained for 45 min at 4 °C. The first sample was mixed with 1 drop of compensation beads (OneComp eBeads, Invitrogen #01-1111) and stained with CD34 (mouse anti-human IgG1, BD Biosciences #560940) and CD31 (mouse anti-human IgG, BD Biosciences #564630), with wash and resuspension into 1 mL PBS + 2% FBS following staining. The second sample was stained with PI (viability dye) (anti-all species, BD Biosciences #556463). A BDFACSAria II SORP cell sorter by the Flow Cytometry Lab in the McGowan Institute of Regenerative Medicine (University of Pittsburgh, PA) demonstrated a distribution of cell markers (Fig. 6D).

4.5 qRT-PCR.

Following sonication of frozen fibrin gel constructs, RNA collection was performed using an illustra RNAspin Mini Kit (GE Healthcare Life Sciences, #25050070) and RNA concentration quantification was performed by spectrophotometry at 260 and 280 nm (BioTek Take3 micro-volume plate). After pre-heating template (65°C, 5 minutes), synthesis of first-strand cDNA was performed using the SuperScript IV First-Strand Synthesis System (Invitrogen #18091050) (23°C/10 minutes, 55°C/10 minutes, 80°C/10 minutes). RT-qPCR was performed using KiCqStart SYBR Green ReadyMix with ROX (Sigma-Aldrich # KCQS02), and forward/reverse primers for tropoelastin, fibrillin-1, fibulin-4, fibulin-5, LOX, LOXL-1, LTBP-4, and reference gene GAPDH (see Table for primer sequences) Post-amplification melt curves were used to validate proper amplification.

4.6 Immunostaining and multiphoton imaging.

Constructs were fixed using 2% paraformaldehyde. Immunostaining for elastin (primary: rabbit polyclonal anti-human aortic elastin, Elastin Products Company, 1:1000 dilution; secondary: goat anti-rabbit IgG fluorescein conjugated, Rockland Immunochemicals, 1:750 dilution) and DAPI (ThermoFisher Scientific #D1306) to identify cell nuclei was conducted using confocal microscopy (Olympus Fluoview FV1000 with XLPlan N25X water objective, NA = 1.05) and reconstructed using brightest-pixel z-stack composite (FIJI, public domain). For multiphoton (no immunostaining) imaging, a Zeiss Plan-Apochromat 20× objective (NA = 0.8, WD = 0.55 mm) was used with a glass concave microscope slide (ThermoFisher Scientific, #1519006) with samples submerged in PBS. Samples were excited at a wavelength of 780 nm, with a constant laser power of 1.35 mW and a depth step-size of 2 μm. These methods are similar to previous reports [[93], [94], [95]].

4.7 Ninhydrin (insoluble elastin) and hydroxyproline (collagen) assays.

Fibrin gel constructs, frozen at −80 °C following culture without fixation, were thawed immediately before base hydrolysis (0.1 M NaOH, 1 h, 98 °C) and subsequent centrifugation to separate insoluble elastin protein from soluble non-elastin protein [57]. Acid hydrolysis (6 N HCl, 24 h, 110 °C) and assay quantification on both soluble and insoluble fractions (ninhydrin-based for elastin, hydroxyproline-based for collagen) allow for protein deposition quantification within each 3D construct.

4.8 Tensile testing of soft substrate fibrin gel constructs.

Constructs were harvested, without fixation, by cutting the pair of nylon tabs within the Linear TissueTrain plates to keep each gel intact. The nylon tabs of each sample were

isolated from the fibrin gel constructs, dried, and secured in compression-based pneumatic clamps lined with sandpaper to improve grip fidelity [48,96] (Fig. 6A). Pure tensile testing was performed on all samples as all sample width-to-length ratios were <0.25:1 (mean = 0.17 ± 0.05, range: 0.12–0.23) [97].

A uniaxial tensile testing device (Instron, #5543A, Norwood, MA) was used to assess the tensile mechanical properties of the strands (Fig. 6B). The thickness (average: 2.17 ± 0.32 mm NT vs 2.06 ± 0.41 mm ASC-SF), width (average: 2.55 ± 0.47 mm NT vs 2.53 ± 0.54 mm ASC-SF), and gauge length (average: 15.47 ± 1.05 mm NT vs 13.99 ± 1.81 mm ASC-SF) of the samples were measured using photos obtained after 0.01 N pre-loading to eliminate sample slack (Fig. 6B) (FIJI, public domain).

A constant 0.1 mm/s crosshead speed extension was used until failure to characterize the mechanical behavior of the samples under quasi-static loading [98]. Force and displacement values were recorded throughout the test and converted to stress-stretch ratio plots [99], where – Stretch ratio: $\lambda = L / Lo$; stress $\sigma = F / Ao$. These measurements were calculated from the sample gauge length in the loaded (L) and unloaded configuration (Lo), along with the force (F) and original cross-sectional area (Ao) recorded during each mechanical test.

Low- and high-stretch moduli are defined as the slope of the linear portion of the mechanical response curve in the low and high stretch regions respectively, in line with previous work [100]. The transition between the low and high stretch regions is defined as the point of the stress–stretch ratio curve with the maximum normal distance from the global secant, which is the line spanning from the origin to the end of the curve [85,101]. This translated to dividing the curves into three equal parts and treating the

initial and final thirds of the curve as the low and high stretch regions respectively. The low stretch region ranged from 1 to 1.13 ± 0.02 for both the ASC-SF the NT groups, and 1 to 1.16 ± 0.04 for the blank gels. The high stretch region ranged from 1.26 ± 0.04 to 1.39 ± 0.06 for the ASC-SF group, 1.26 ± 0.04 to 1.4 ± 0.06 for the NT group and 1.32 ± 0.07 to 1.49 ± 0.11 for the blank gels.

4.9 Statistical Analysis

Means comparisons were conducted using individual t-tests or one-way ANOVA with Tukey post-hoc tests, as appropriate. Significance threshold of $\alpha = 0.05$ was set for all presented data, with experimental sample size of tested constructs listed on each figure. IBM SPSS was used for all statistical analysis. All displayed data values written after "±" are Standard Deviation values. "n" numbers all refer to number of fibrin gel samples for each experiment.

Sources of funding:

This work was supported by the Leonard H. Berenfield Graduate Fellowship in Cardiovascular Bioengineering and NIH T32 HL094295 (fellowships to A.K.R.), the University of Pittsburgh's International Studies Fund (to R.E.S.), the European Union's Horizon 2020 - Research and Innovation Framework Program under the H2020 Marie Skłodowska-Curie Actions grant 708867 (to E.M.C.), the NIH grants HL129066 and HL130784 and McCune Foundation Pediatric Device Initiative (to D.A.V.), and University of Pittsburgh Competitive Medical Research Fund (to J.S.W.).

Table: RT-qPCR Primers

Gene	Forward Primer	Reverse Primer
Tropoelastin	CCAAGGTGGCTGCCAAAG	GACGCCGACACCAACTCC
Fibrillin-1	AGCGGAGCCGAGCAGTGG	GCTGCTCCCACTTCAGGC
LTBP-4	AGCGTTGCTGTTTGTCGCTG	TTGAGGGACACCTGTCTCTTC
Fibulin-4	GCTTCTCCTGCAGTGATATTGAT	CTGACGTTGTTGATTTGCCTAA
Fibulin-5	TTCCTCTGCCAACATGAGTG	TGGTTCCTGTGCTCACATTC
LOX	CATAGACTGCCAGTGGATTGA	ATGTCACAGCGCACAACATT
LOXL-1	AGCGCTATGCATGCACCTCTCATA	TGCAGAAACGTAGCGACCTGTGTA
GAPDH	CCACCCAGAAGACTGTGGAT	TTCAGCTCAGGGATGACCTT

Figure Captions:

Figure 1: SMC elastogenesis cascade. (1) Transcription of tropoelastin and its chaperone organizational matricellular proteins. (2) Tropoelastin and chaperone proteins assemble outside of the cell, with two major classes of interactions. One is mediated by fibulin-4, which binds to tropoelastin and facilitates cross-linking by lysyl oxidase (LOX). The other is mediated by fibulin-5, which binds tropoelastin together with lysyl oxidase-like 1 (LOXL-1). (3) Tropoelastin coacervates, or globules of tropoelastin and chaperone proteins, are formed. (4) Tropoelastin coacervates are deposited along the fibrillin-1 microfibril complex, with initial interaction mediated by LTBP-4. Note that many important steps of microfibril assembly prior to elastin deposition, including the involvement of fibronectin, are excluded here for clarity. (5) Deposited tropoelastin coacervates integrate within the fibrillin-1/LTBP-1/LTBP-2/fibronectin microfibril complex. (6) Cross-linking, via LOX and LOXL-1, occurs between deposited tropoelastin coacervates within the microfibril complex, opening the coacervate structure and

forming mature, mechanically-competent elastic fibers. Illustration credit: Rick Henkel at Light House Artwork (rick@lighthouseartwork.com).

Figure 2: SMC transcriptional changes after 30 days of ASC-SF stimulation of SMCs. (A) Gene expression related to SMC phenotype. RT-qPCR revealed an increase in myosin heavy chain (MYH11) after ASC-SF stimulation, while both α smooth muscle actin (ACTA2) and calponin (CAL) were unchanged. n = 3. (B) Gene expression related to elastic fiber formation. RT-qPCR revealed increases in expression of tropoelastin induced by both ASC-SF and NCM, as well as ASC-SF induced increases in microfibril protein fibrillin-1, organizational matricellular protein fibulin-5, and cross-linking proteins lysyl oxidase (LOX) and lysyl oxidase-like 1 (LOXL-1). Fibulin-4 expression was unchanged with both ASC-SF stimulation and NCM when compared to NT, and LTBP-4 expression was significantly reduced with both ASC-SF stimulation and NCM.

Figure 3: Induction of elastic fiber deposition by ASC-SF, as revealed by immunofluorescence and multiphoton microscopy. SMC elastic fibers (green) were revealed after ASC-SF stimulation (B), when compared to both No Treatment (A, NT) and Non-Conditioned Media (C, NCM) negative controls, in sample images of z-stacked confocal images of 30-day discs. Note that cellularity (nuclear stain, blue) is similar among groups. Separate discs were then analyzed by multiphoton microscopy using a Zeiss Plan-Apochromat 20× objective. (D) Composite image (1 × 5) of a representative NT control disc. (E) Composite image (2 × 5) of a representative ASC-SF stimulated disc. Arrows indicate areas of elastic fiber autofluorescence, and inset illustrates detail of elastic fibers. (F) Composite image (2 × 5) of a representative NCM-stimulated disc. All scale bars = 100 μm.

Figure 4: Insoluble elastin and collagen are enhanced by ASC-SF stimulation of SMCs, under varying geometries and loading conditions. (A–D) Discs were analyzed for (A) insoluble elastin percentage of total protein, (B) insoluble elastin per disc, (C) collagen percentage of total protein, and (D) collagen per disc, comparing control NT and NCM treatments with ASC-SF stimulation. (C, F) Strands were analyzed for (C) insoluble elastin percentage and (F) collagen percentage of total protein, comparing NT control treatment to ASC-SF stimulation under constrained and dynamic loading conditions.

Figure 5: Shift in strand mechanical properties after ASC-SF stimulation. (A) Photo of fibrin removed from top half of nylon tabs of TissueTrain plates, resulting in an exposed tab that can be dried and clamped by sandpaper-aided pneumatic clamps. (B) Image of tensile testing configuration (Instron #5543A, with sandpaper-lined pneumatic clamps) used to test 30-day NT and ASC-SF treated strands, with ruler for scale. (C) For each sample group, the range of maximum and minimum stress values was plotted as a pair of thick lines, with the average values plotted as small circles. “Low” and “High” stretch regions are indicated, for each sample this was the first and final 1/3 of data points, respectively. (D) Comparison of low and high stretch elastic modulus for both 30-day NT and ASC-SF stimulated strands, alongside cell-free fibrin gel constructs.

Figure 6: Three-dimensional fibrin gel culture constructs and ASC-SF collection. (A) Fibrin gel “discs” (200 µL), plated on 24-well tissue culture plates within 7.94 mm diameter heat-stamped templates. (B) Fibrin gel “strands” (600 µL), plated between nylon tabs of FlexCell Linear TissueTrain untreated plates. Note that the discs are cultured on top of stiff tissue culture plastic while strands are cultured on top of a flexible

silicone membrane. In the schematic, the long dimension is shown to illustrate the direction of constraint and dynamic stretch, however the overall geometry differs from a disc (see top view in photo). (C) ASC isolation following body-sculpting surgeries of non-smoking, non-diabetic patients below 45 years old. Stromal vascular fraction (SVF) is obtained following adipose tissue mincing and collagenase digestion, and ASCs are cultured within standard tissue culture flasks. Conditioned media (ASC-CM) is collected every 24–72 h in culture, from passages 0 to 1. (D) ASCs were sorted by flow cytometry according to staining for CD31 and CD34 cell markers, and then quantified according to percent in each subpopulation. Note the predominance of CD34+/CD31− cells (87%) among the ASCs used for media conditioning.

References

[1] D.M. Milewicz, D.C. Guo, V. Tran-Fadulu, A.L. Lafont, C.L. Papke, S. Inamoto, C.S. Kwartler, H. Pannu Genetic basis of thoracic aortic aneurysms and dissections: focus on smooth muscle cell contractile dysfunction Annu. Rev. Genomics Hum. Genet., 9 (2008), pp. 283-302

[2] C. Fleming, E.P. Whitlock, T.L. Bell, F.A. Lederle Screening for abdominal aortic aneurysm: a best-evidence systematic review for the US Preventive Services Task Force Ann. Intern. Med., 142 (3) (2005), pp. 203-211

[3] E. Gillis, L. Van Laer, B.L. Loeys Genetics of thoracic aortic aneurysm: at the crossroad of transforming growth factor-beta signaling and vascular smooth muscle cell contractility Circ. Res., 113 (3) (2013), pp. 327-340

[4] K.C. Kent, R.M. Zwolak, N.N. Egorova, T.S. Riles, A. Manganaro, A.J. Moskowitz, A.C. Gelijns, G. Greco Analysis of risk factors for abdominal aortic aneurysm in a cohort of more than 3 million individuals J. Vasc. Surg., 52 (3) (2010), pp. 539-548

[5] K.C. Kent Clinical practice Abdominal aortic aneurysms, N Engl J Med, 371 (22) (2014), pp. 2101-2108

[6] L.L. Hoornweg, M.N. Storm-Versloot, D.T. Ubbink, M.J. Koelemay, D.A. Legemate, R. Balm Meta analysis on mortality of ruptured abdominal aortic aneurysms Eur. J. Vasc. Endovasc. Surg., 35 (5) (2008), pp. 558-570

[7] N. Kontopodis, D. Pantidis, A. Dedes, N. Daskalakis, C.V. Ioannou, The-not so-solid 5.5 cm threshold for abdominal aortic aneurysm repair: facts, misinterpretations, and future directions, Front Surg 3 (2016) 1.

[8] W.H. Pearce, C.K. Zarins, J.M. Bacharach, G. American Heart Association Writing, Atherosclerotic Peripheral Vascular Disease Symposium II: controversies in abdominal aortic aneurysm repair, Circulation 118(25) (2008) 2860–3.

[9] Underlying Cause of Death 1999–2016 on CDC WONDER Online Database, released December 2017., in: N.C.f.H.S. Centers for Disease Control and Prevention (Ed.) Vital Statistics Cooperative Program. 2017.

[10] C.M. Kelleher, S.E. McLean, R.P. Mecham Vascular extracellular matrix and aortic development Curr. Top. Dev. Biol., 62 (2004), pp. 153-188

[11] B. Saitow Cassandra, G. Wise Steven, S. Weiss Anthony, J. Castellot John, L. Kaplan David, Elastin biology and tissue engineering with adult cells, BioMolecular Concepts, 2013, p. 173.

[12] J.D. Humphrey, G.A. Holzapfel Mechanics, mechanobiology, and modeling of human abdominal aorta and aneurysms J. Biomech., 45 (5) (2012), pp. 805-814

[13] D.A. Vorp Biomechanics of abdominal aortic aneurysm J. Biomech., 40 (9) (2007), pp. 1887-1902

[14] A. Tsamis, J.T. Krawiec, D.A. Vorp Elastin and collagen fibre microstructure of the human aorta in ageing and disease: a review J. R. Soc. Interface, 10 (83) (2013), p. 20121004

[15] G.M. Longo, W. Xiong, T.C. Greiner, Y. Zhao, N. Fiotti, B.T. Baxter Matrix metalloproteinases 2 and 9 work in concert to produce aortic aneurysms J. Clin. Invest., 110 (5) (2002), pp. 625-632

[16] K. Shimizu, R.N. Mitchell, P. Libby Inflammation and cellular immune responses in abdominal aortic aneurysms Arterioscler. Thromb. Vasc. Biol., 26 (5) (2006), pp. 987-994

[17] G. Ailawadi, J.L. Eliason, G.R. Upchurch Jr. Current concepts in the pathogenesis of abdominal aortic aneurysm J. Vasc. Surg., 38 (3) (2003), pp. 584-588

[18] M.E. Lindsay, H.C. Dietz Lessons on the pathogenesis of aneurysm from heritable conditions Nature, 473 (7347) (2011), pp. 308-316

[19] A. LopezCandales, D.R. Holmes, S.X. Liao, M.J. Scott, S.A. Wickline, R.W. Thompson Decreased vascular smooth muscle cell density in medial degeneration of human abdominal aortic aneurysms Am. J. Pathol., 150 (3) (1997), pp. 993-1007

[20] L.A. Pape, T.T. Tsai, E.M. Isselbacher, J.K. Oh, T. O'Gara P, A. Evangelista, R. Fattori, G. Meinhardt, S. Trimarchi, E. Bossone, T. Suzuki, J.V. Cooper, J.B. Froehlich, C.A. Nienaber, K.A. Eagle, I. International Registry of Acute Aortic Dissection, Aortic diameter > or =5.5 cm is not a good predictor of type A aortic dissection: observations from the International Registry of Acute Aortic Dissection (IRAD), Circulation 116(10) (2007) 1120–7.

[21] B.T. Baxter, M.C. Terrin, R.L. Dalman Medical management of small abdominal aortic aneurysms Circulation, 117 (14) (2008), pp. 1883-1889

[22] A.S. Chun, J.A. Elefteriades, S.K. Mukherjee Do beta-blockers really work for prevention of aortic aneurysms?: time for reassessment Aorta (Stamford), 1 (1) (2013), pp. 45-51

[23] S.C. Nicholls, J.B. Gardner, M.H. Meissner, H.K. Johansen Rupture in small abdominal aortic aneurysms J. Vasc. Surg., 28 (5) (1998), pp. 884-888

[24] M.J. Sweeting, S.G. Thompson, L.C. Brown, R.M. Greenhalgh, J.T. Powell Use of angiotensin converting enzyme inhibitors is associated with increased growth rate of abdominal aortic aneurysms J. Vasc. Surg., 52 (1) (2010), pp. 1-4

[25] A.C. Braverman Medical management of thoracic aortic aneurysm disease J. Thorac. Cardiovasc. Surg., 145 (3 Suppl) (2013), pp. S2-S6

[26] K. McGee, E. Bollache, A.J. Barker, J.C. Carr, M. Markl, P. Kansal Impact of beta-blocker, ACE inhibitor, and ARB therapy on thoracic aorta wall shear stress in bicuspid aortic valve patients J. Cardiovasc. Magn. Reson., 18 (S1) (2016), p. P345

[27] K.J. Blose, T.L. Ennis, B. Arif, J.S. Weinbaum, J.A. Curci, D.A. Vorp Periadventitial adipose-derived stem cell treatment halts elastase-induced abdominal aortic aneurysm progression Regen. Med., 9 (6) (2014), pp. 733-741

[28] L. Lin, L. Du The role of secreted factors in stem cells-mediated immune regulation Cell. Immunol., 326 (2018), pp. 24-32

[29] G. Swaminathan, V.S. Gadepalli, I. Stoilov, R.P. Mecham, R.R. Rao, A. Ramamurthi Pro-elastogenic effects of bone marrow mesenchymal stem cell-derived smooth muscle cells on cultured aneurysmal smooth muscle cells J. Tissue Eng. Regen. Med., 11 (3) (2017), pp. 679-693

[30] G. Swaminathan, I. Stoilov, T. Broekelmann, R. Mecham, A. Ramamurthi Phenotype-based selection of bone marrow mesenchymal stem cell-derived smooth muscle cells for elastic matrix regenerative repair in abdominal aortic aneurysms J. Tissue Eng. Regen. Med., 12 (1) (2018), pp. e60-e70

[31] P.C. Baer Adipose-derived mesenchymal stromal/stem cells: an update on their phenotype in vivo and in vitro World J Stem Cells, 6 (3) (2014), pp. 256-265

[32] J.T. Krawiec, J.S. Weinbaum, C.M. St Croix, J.A. Phillippi, S.C. Watkins, J.P. Rubin, D.A. Vorp A cautionary tale for autologous vascular tissue engineering: impact of human demographics on the ability of adipose-derived mesenchymal stem cells to recruit and differentiate into smooth muscle cells Tissue Eng. A, 21 (3–4) (2015), pp. 426-437

[33] J.D. Roh, R. Sawh-Martinez, M.P. Brennan, S.M. Jay, L. Devine, D.A. Rao, T. Yi, T.L. Mirensky, A. Nalbandian, B. Udelsman, N. Hibino, T. Shinoka, W.M. Saltzman, E. Snyder, T.R. Kyriakides, J.S. Pober, C.K. Breuer Tissue-engineered vascular grafts transform into mature blood vessels via an inflammation-mediated process of vascular remodeling Proc. Natl. Acad. Sci. U. S. A., 107 (10) (2010), pp. 4669-4674

[34] A.I. Hoch, B.Y. Binder, D.C. Genetos, J.K. Leach Differentiation-dependent secretion of proangiogenic factors by mesenchymal stem cells PLoS One, 7 (4) (2012), Article e35579

[35] G.E. Kilroy, S.J. Foster, X. Wu, J. Ruiz, S. Sherwood, A. Heifetz, J.W. Ludlow, D.M. Stricker, S. Potiny, P. Green, Y.D. Halvorsen, B. Cheatham, R.W. Storms, J.M. Gimble Cytokine profile of human adipose-derived stem cells: expression of angiogenic, hematopoietic, and pro-inflammatory factors J. Cell. Physiol., 212 (3) (2007), pp. 702-709

[36] S. Wang, M. Tong, S. Hu, X. Chen The bioactive substance secreted by MSC retards mouse aortic vascular smooth muscle cells calcification Biomed. Res. Int., 2018 (2018), p. 6053567

[37] J.J. Ross, R.T. Tranquillo ECM gene expression correlates with in vitro tissue growth and development in fibrin gel remodeled by neonatal smooth muscle cells Matrix Biol., 22 (6) (2003), pp. 477-490

[38] J.L. Long, R.T. Tranquillo Elastic fiber production in cardiovascular tissue-equivalents Matrix Biol., 22 (4) (2003), pp. 339-350

[39] S. Hinderer, N. Shena, L.J. Ringuette, J. Hansmann, D.P. Reinhardt, S.Y. Brucker, E.C. Davis, K. Schenke-Layland In vitro elastogenesis: instructing human vascular smooth muscle cells to generate an elastic fiber-containing extracellular matrix scaffold Biomed. Mater., 10 (3) (2015), Article 034102

[40] C.L. Papke, H. Yanagisawa Fibulin-4 and fibulin-5 in elastogenesis and beyond: insights from mouse and human studies Matrix Biol., 37 (2014), pp. 142-149

[41] M. Hirai, T. Ohbayashi, M. Horiguchi, K. Okawa, A. Hagiwara, K.R. Chien, T. Kita, T. Nakamura Fibulin-5/DANCE has an elastogenic organizer activity that is abrogated by proteolytic cleavage in vivo J. Cell Biol., 176 (7) (2007), pp. 1061-1071

[42] K. Noda, B. Dabovic, K. Takagi, T. Inoue, M. Horiguchi, M. Hirai, Y. Fujikawa, T.O. Akama, K. Kusumoto, L. Zilberberg, L.Y. Sakai, K. Koli, M. Naitoh, H. von Melchner, S. Suzuki, D.B. Rifkin, T. Nakamura Latent TGF-beta binding protein 4 promotes elastic fiber assembly by interacting with fibulin-5 Proc. Natl. Acad. Sci. U. S. A., 110 (8) (2013), pp. 2852-2857

[43] I. Bultmann-Mellin, A. Conradi, A.C. Maul, K. Dinger, F. Wempe, A.P. Wohl, T. Imhof, F.T. Wunderlich, A.C. Bunck, T. Nakamura, K. Koli, W. Bloch, A. Ghanem, A. Heinz, H. von Melchner, G. Sengle, A. Sterner-Kock Modeling autosomal recessive cutis laxa type 1C in mice reveals distinct functions for Ltbp-4 isoforms Dis. Model. Mech., 8 (4) (2015), pp. 403-415

[44] I.B. Robertson, M. Horiguchi, L. Zilberberg, B. Dabovic, K. Hadjiolova, D.B. Rifkin

Latent TGF-beta-binding proteins Matrix Biol., 47 (2015), pp. 44-53

[45] E. El-Hallous, T. Sasaki, D. Hubmacher, M. Getie, K. Tiedemann, J. Brinckmann, B. Batge, E.C. Davis, D.P. Reinhardt Fibrillin-1 interactions with fibulins depend on the first hybrid domain and provide an adaptor function to tropoelastin J. Biol. Chem., 282 (12) (2007), pp. 8935-8946

[46] G.M. Northington Fibulin-5: two for the price of one maintaining pelvic support

J. Clin. Invest., 121 (5) (2011), pp. 1688-1691

[47] J. Aziz, H. Shezali, Z. Radzi, N.A. Yahya, N.H. Abu Kassim, J. Czernuszka, M.T. Rahman Molecular mechanisms of stress-responsive changes in collagen and elastin networks in skin Skin Pharmacol. Physiol., 29 (4) (2016), pp. 190-203

[48] K.J. Blose, J.E. Pichamuthu, J.S. Weinbaum, D.A. Vorp Design and validation of a vacuum assisted anchorage for the uniaxial tensile testing of soft materials Soft Mater, 14 (2) (2016), pp. 72-77

[49] J.E. Wagenseil, R.P. Mecham Elastin in large artery stiffness and hypertension J. Cardiovasc. Transl. Res., 5 (3) (2012), pp. 264-273

[50] N.E. Calabro, A. Barrett, A. Chamorro-Jorganes, S. Tam, N.J. Kristofik, H. Xing, A.M. Loye, W.C. Sessa, K. Hansen, T.R. Kyriakides Thrombospondin-2 regulates extracellular matrix production, LOX levels, and cross-linking via downregulation of miR-29, Matrix Biol (2019)

[51] C.S. Craft, T.J. Broekelmann, R.P. Mecham Microfibril-associated glycoproteins MAGP-1 and MAGP-2 in disease Matrix Biol., 71-72 (2018), pp. 100-111

[52] V.D. Ramaswamy AK, Weinbaum JS, Functional vascular tissue engineering inspired by matricellular proteins, Front. Cardiovasc. Med. (accepted for publication) (2019).

[53] R.C. Deller, T. Richardson, R. Richardson, L. Bevan, I. Zampetakis, F. Scarpa, A.W. Perriman Artificial cell membrane binding thrombin constructs drive in situ fibrin hydrogel formation Nat. Commun., 10 (1) (2019), p. 1887

[54] S. Nandi, E.P. Sproul, K. Nellenbach, M. Erb, L. Gaffney, D.O. Freytes, A.C. Brown Platelet-like particles dynamically stiffen fibrin matrices and improve wound healing outcomes Biomater Sci, 7 (2) (2019), pp. 669-682

[55] O. Adebayo, T.A. Hookway, J.Z. Hu, K.L. Billiar, M.W. Rolle Self-assembled smooth muscle cell tissue rings exhibit greater tensile strength than cell-seeded fibrin or collagen gel rings J. Biomed. Mater. Res. A, 101 (2) (2013), pp. 428-437

[56] J.L. Grouf, A.M. Throm, J.L. Balestrini, K.A. Bush, K.L. Billiar Differential effects of EGF and TGF-beta1 on fibroblast activity in fibrin-based tissue equivalents Tissue Eng., 13 (4) (2007), pp. 799-807

[57] K.A. Ahmann, J.S. Weinbaum, S.L. Johnson, R.T. Tranquillo Fibrin degradation enhances vascular smooth muscle cell proliferation and matrix deposition in fibrin-based tissue constructs fabricated in vitro Tissue Eng. A, 16 (10) (2010), pp. 3261-3270

[58] Z.H. Syedain, L.A. Meier, J.W. Bjork, A. Lee, R.T. Tranquillo Implantable arterial grafts from human fibroblasts and fibrin using a multi-graft pulsed flow-stretch bioreactor with noninvasive strength monitoring Biomaterials, 32 (3) (2011), pp. 714-722

[59] Z.H. Syedain, J.S. Weinberg, R.T. Tranquillo Cyclic distension of fibrin-based tissue constructs: evidence of adaptation during growth of engineered connective tissue Proc. Natl. Acad. Sci. U. S. A., 105 (18) (2008), pp. 6537-6542

[60] L.D. Black 3rd, J.D. Meyers, J.S. Weinbaum, Y.A. Shvelidze, R.T. Tranquillo Cell-induced alignment augments twitch force in fibrin gel-based engineered myocardium via gap junction modification Tissue Eng. A, 15 (10) (2009), pp. 3099-3108

[61] C. Williams, E. Budina, W.L. Stoppel, K.E. Sullivan, S. Emani, S.M. Emani, L.D. Black 3rd Cardiac extracellular matrix-fibrin hybrid scaffolds with tunable properties for cardiovascular tissue engineering Acta Biomater., 14 (2015), pp. 84-95

[62] E.D. Grassl, T.R. Oegema, R.T. Tranquillo A fibrin-based arterial media equivalent

J. Biomed. Mater. Res. A, 66 (3) (2003), pp. 550-561

[63] E. Chung, J.A. Rytlewski, A.G. Merchant, K.S. Dhada, E.W. Lewis, L.J. Suggs Fibrin-based 3D matrices induce angiogenic behavior of adipose-derived stem cells Acta Biomater., 17 (2015), pp. 78-88

[64] G. Zhang, X. Wang, Z. Wang, J. Zhang, L. Suggs A PEGylated fibrin patch for mesenchymal stem cell delivery Tissue Eng., 12 (1) (2006), pp. 9-19

[65] M.S. Liang, S.T. Andreadis Engineering fibrin-binding TGF-beta1 for sustained signaling and contractile function of MSC based vascular constructs Biomaterials, 32 (33) (2011), pp. 8684-8693

[66] D.D. Swartz, J.A. Russell, S.T. Andreadis Engineering of fibrin-based functional and implantable small-diameter blood vessels Am. J. Physiol. Heart Circ. Physiol., 288 (3) (2005), pp. H1451-H1460

[67] L. Yao, J. Liu, S.T. Andreadis Composite fibrin scaffolds increase mechanical strength and preserve contractility of tissue engineered blood vessels Pharm. Res., 25 (5) (2008), pp. 1212-1221

[68] S. Jockenhoevel, G. Zund, S.P. Hoerstrup, K. Chalabi, J.S. Sachweh, L. Demircan, B.J. Messmer, M. Turina Fibrin gel — advantages of a new scaffold in cardiovascular tissue engineering Eur. J. Cardiothorac. Surg., 19 (4) (2001), pp. 424-430

[69] H. Hong, J.P. Stegemann 2D and 3D collagen and fibrin biopolymers promote specific ECM and integrin gene expression by vascular smooth muscle cells J Biomater Sci Polym Ed, 19 (10) (2008), pp. 1279-1293

[70] M.K. Proulx, S.P. Carey, L.M. Ditroia, C.M. Jones, M. Fakharzadeh, J.P. Guyette, A.L. Clement, R.G. Orr, M.W. Rolle, G.D. Pins, G.R. Gaudette Fibrin microthreads support mesenchymal stem cell growth while maintaining differentiation potential J. Biomed. Mater. Res. A, 96 (2) (2011), pp. 301-312

[71] A.W. Peterson, D.J. Caldwell, A.Y. Rioja, R.R. Rao, A.J. Putnam, J.P. Stegemann Vasculogenesis and angiogenesis in modular collagen-fibrin microtissues Biomater Sci, 2 (10) (2014), pp. 1497-1508

[72] O.V. Sazonova, B.C. Isenberg, J. Herrmann, K.L. Lee, A. Purwada, A.D. Valentine, J.A. Buczek-Thomas, J.Y. Wong, M.A. Nugent Extracellular matrix presentation modulates vascular smooth muscle cell mechanotransduction Matrix Biol., 41 (2015), pp. 36-43

[73] X.Q. Brown, E. Bartolak-Suki, C. Williams, M.L. Walker, V.M. Weaver, J.Y. Wong Effect of substrate stiffness and PDGF on the behavior of vascular smooth muscle cells: implications for atherosclerosis J. Cell. Physiol., 225 (1) (2010), pp. 115-122

[74] J.L. Balestrini, K.L. Billiar Equibiaxial cyclic stretch stimulates fibroblasts to rapidly remodel fibrin J. Biomech., 39 (16) (2006), pp. 2983-2990

[75] T.C. Flanagan, C. Cornelissen, S. Koch, B. Tschoeke, J.S. Sachweh, T. Schmitz-Rode, S. Jockenhoevel The in vitro development of autologous fibrin-based tissue-engineered heart valves through optimised dynamic conditioning Biomaterials, 28 (23) (2007), pp. 3388-3397

[76] J.S. Weinbaum, J.B. Schmidt, R.T. Tranquillo Combating adaptation to cyclic stretching by prolonging activation of extracellular signal-regulated kinase Cell. Mol. Bioeng., 6 (3) (2013), pp. 279-286

[77] M. Yamauchi, Y. Taga, S. Hattori, M. Shiiba, M. Terajima Analysis of collagen and elastin cross-links Methods Cell Biol., 143 (2018), pp. 115-132

[78] M.L. Duque Lasio, B.A. Kozel Elastin-driven genetic diseases Matrix Biol., 71-72 (2018), pp. 144-160

[79] R.P. Mecham Elastin in lung development and disease pathogenesis Matrix Biol., 73 (2018), pp. 6-20

[80] M.J. Collins, J.F. Eberth, E. Wilson, J.D. Humphrey Acute mechanical effects of elastase on the infrarenal mouse aorta: implications for models of aneurysms J. Biomech., 45 (4) (2012), pp. 660-665

[81] G. Holzapfel Biomechanics of Soft Tissue (2001)

[82] A. Hemmasizadeh, A. Tsamis, R. Cheheltani, S. Assari, A. D'Amore, M. Autieri, M.F. Kiani, N. Pleshko, W.R. Wagner, S.C. Watkins, D. Vorp, K. Darvish Correlations between transmural mechanical and morphological properties in porcine thoracic descending aorta J. Mech. Behav. Biomed. Mater., 47 (2015), pp. 12-20

[83] Y. Huo, Y. Cheng, X. Zhao, X. Lu, G.S. Kassab Biaxial vasoactivity of porcine coronary artery Am. J. Physiol. Heart Circ. Physiol., 302 (10) (2012), pp. H2058-H2063

[84] A.J. Ryan, F.J. O'Brien Insoluble elastin reduces collagen scaffold stiffness, improves viscoelastic properties, and induces a contractile phenotype in smooth muscle cells Biomaterials, 73 (2015), pp. 296-307

[85] G.A. Holzapfel Determination of material models for arterial walls from uniaxial extension tests and histological structure J. Theor. Biol., 238 (2) (2006), pp. 290-302

[86] S. Menashi, J.S. Campa, R.M. Greenhalgh, J.T. Powell Collagen in abdominal aortic aneurysm: typing, content, and degradation J. Vasc. Surg., 6 (6) (1987), pp. 578-582

[87] S.A. Gharib, A.M. Manicone, W.C. Parks Matrix metalloproteinases in emphysema

Matrix Biol., 73 (2018), pp. 34-51

[88] E.M. Cunnane, J.S. Weinbaum, F.J. O'Brien, D.A. Vorp Future perspectives on the role of stem cells and extracellular vesicles in vascular tissue regeneration Front Cardiovasc Med, 5 (2018), p. 86

[89] H.R. Hofer, R.S. Tuan Secreted trophic factors of mesenchymal stem cells support neurovascular and musculoskeletal therapies Stem Cell Res Ther, 7 (1) (2016), p. 131

[90] X. Tian, J. Fan, M. Yu, Y. Zhao, Y. Fang, S. Bai, W. Hou, H. Tong Adipose stem cells promote smooth muscle cells to secrete elastin in rat abdominal aortic aneurysm PLoS One, 9 (9) (2014), Article e108105

[91] D.G. Haskett, K.S. Saleh, K.L. Lorentz, A.D. Josowitz, S.K. Luketich, J.S. Weinbaum, L.E. Kokai, A. D'Amore, K.G. Marra, J.P. Rubin, W.R. Wagner, D.A. Vorp, An exploratory study on the preparation and evaluation of a “same-day” adipose stem cell-based tissue-engineered vascular graft, J Thorac Cardiovasc Surg 156(5) (2018) 1814–1822 e3.

[92] J.T. Krawiec, H.T. Liao, L.L. Kwan, A. D'Amore, J.S. Weinbaum, J.P. Rubin, W.R. Wagner, D.A. Vorp, Evaluation of the stromal vascular fraction of adipose tissue as the basis for a stem cell-based tissue-engineered vascular graft, J Vasc Surg 66(3) (2017) 883–890 e1.

[93] D. Haskett, M. Azhar, U. Utzinger, J.P. Vande Geest Progressive alterations in microstructural organization and biomechanical response in the ApoE mouse model of aneurysm Biomatter, 3 (3) (2013)

[94] P.S. Gade, A.M. Robertson, C.Y. Chuang Multiphoton imaging of collagen, elastin, and calcification in intact soft-tissue samples Curr Protoc Cytom, 87 (1) (2019), Article e51

[95] S. Sugita, M. Kato, F. Wataru, M. Nakamura Three-dimensional analysis of the thoracic aorta microscopic deformation during intraluminal pressurization Biomech. Model. Mechanobiol. (2019), 10.1007/s10237-019-01201-w

[96] A. Tsamis, J.A. Phillippi, R.G. Koch, S. Pasta, A. D'Amore, S.C. Watkins, W.R. Wagner, T.G. Gleason, D.A. Vorp Fiber micro-architecture in the longitudinal-radial and circumferential-radial planes of ascending thoracic aortic aneurysm media J. Biomech., 46 (16) (2013), pp. 2787-2794

[97] J.J. Mulvihill, M.T. Walsh On the mechanical behaviour of carotid artery plaques: the influence of curve-fitting experimental data on numerical model results Biomech. Model. Mechanobiol., 12 (5) (2013), pp. 975-985

[98] G.A. Holzapfel, G. Sommer, P. Regitnig Anisotropic mechanical properties of tissue components in human atherosclerotic plaques Journal of Biomechanical Engineering-Transactions of the Asme, 126 (5) (2004), pp. 657-665

[99] M.T. Walsh, E.M. Cunnane, J.J. Mulvihill, A.C. Akyildiz, F.J. Gijsen, G.A. Holzapfel Uniaxial tensile testing approaches for characterisation of atherosclerotic plaques J. Biomech., 47 (4) (2014), pp. 793-804

[100] E.J. White, E.M. Cunnane, M. McMahon, M.T. Walsh, J.C. Coffey, L. O'Sullivan Mechanical characterisation of porcine non-intestinal colorectal tissues for innovation in surgical instrument design Proc Inst Mech Eng H, 232 (8) (2018), pp. 796-806

[101] E.M. Cunnane, J.J.E. Mulvihill, H.E. Barrett, M.M. Hennessy, E.G. Kavanagh, M.T. Walsh Mechanical properties and composition of carotid and femoral atherosclerotic plaques: a comparative study J. Biomech., 49 (15) (2016), pp. 3697-3704

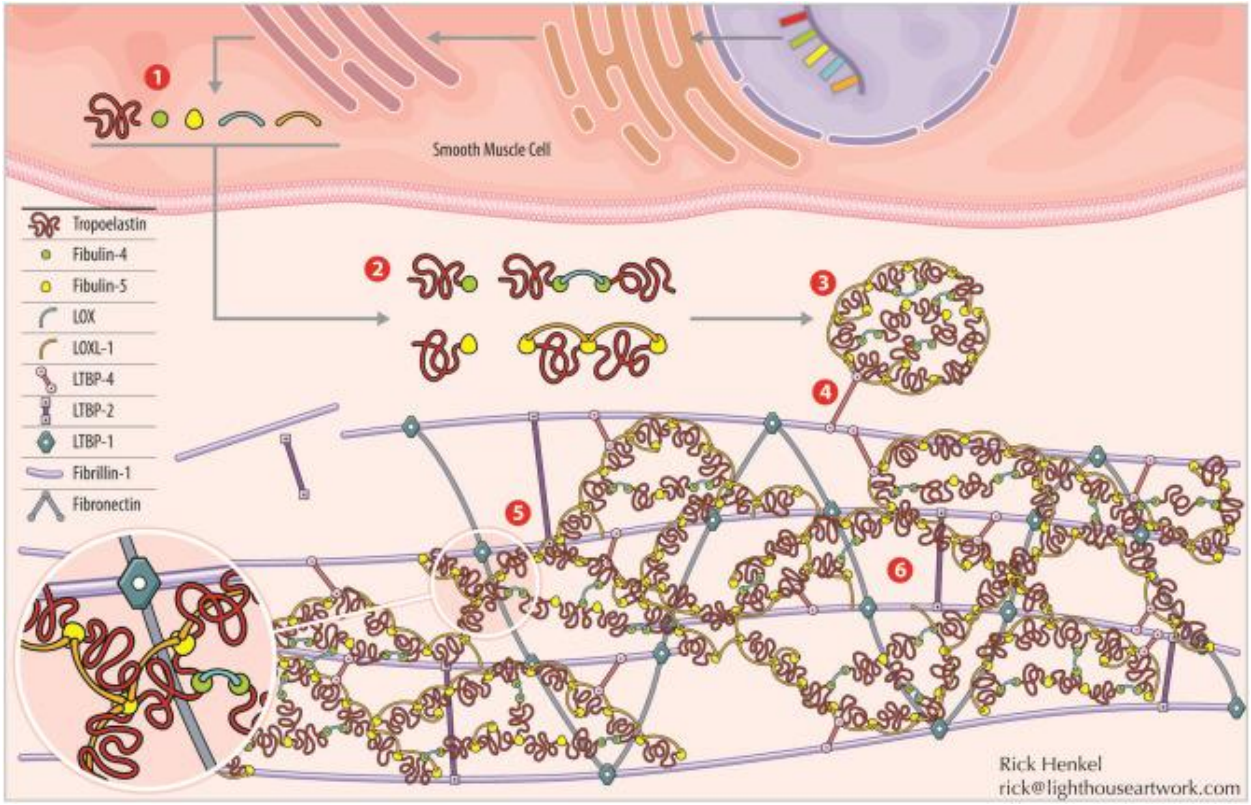

Figure 1: SMC elastogenesis cascade. (1) Transcription of tropoelastin and its chaperone organizational matricellular proteins. (2) Tropoelastin and chaperone proteins assemble outside of the cell, with two major classes of interactions. One is mediated by fibulin-4, which binds to tropoelastin and facilitates cross-linking by lysyl oxidase (LOX). The other is mediated by fibulin-5, which binds tropoelastin together with lysyl oxidase-like 1 (LOXL-1). (3) Tropoelastin coacervates, or globules of tropoelastin and chaperone proteins, are formed. (4) Tropoelastin coacervates are deposited along the fibrillin-1 microfibril complex, with initial interaction mediated by LTBP-4. Note that many important steps of microfibril assembly prior to elastin deposition, including the involvement of fibronectin, are excluded here for clarity. (5) Deposited tropoelastin coacervates integrate within the fibrillin-1/LTBP-1/LTBP-2/fibronectin microfibril complex. (6) Cross-linking, via LOX and LOXL-1, occurs between deposited tropoelastin coacervates within the microfibril complex, opening the coacervate structure and forming mature, mechanically-competent elastic fibers. Illustration credit: Rick Henkel at Light House Artwork (rick@lighthouseartwork.com).

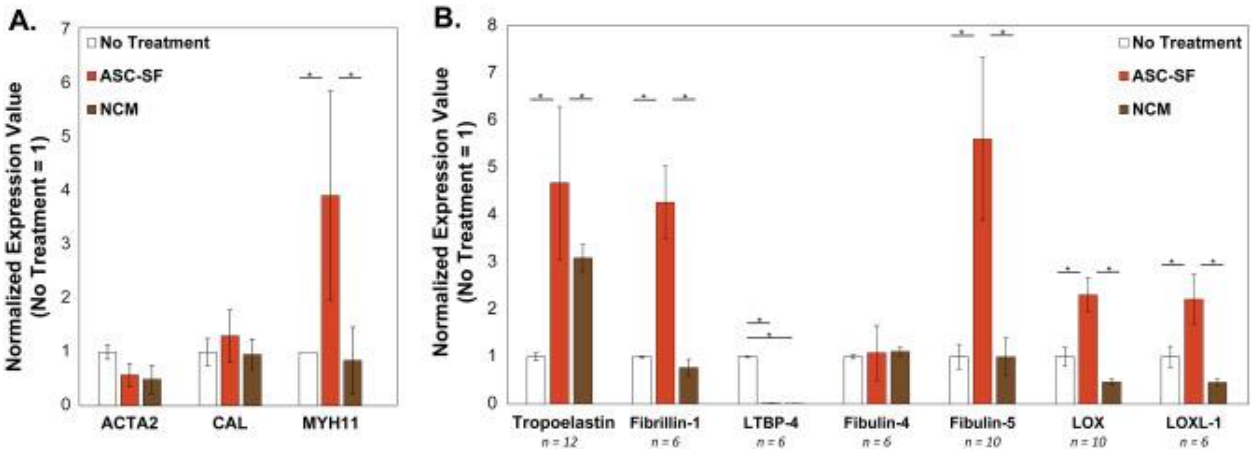

Figure 2: SMC transcriptional changes after 30 days of ASC-SF stimulation of SMCs. (A) Gene expression related to SMC phenotype. RT-qPCR revealed an increase in myosin heavy chain (MYH11) after ASC-SF stimulation, while both α smooth muscle actin (ACTA2) and calponin (CAL) were unchanged. n = 3. (B) Gene expression related to elastic fiber formation. RT-qPCR revealed increases in expression of tropoelastin induced by both ASC-SF and NCM, as well as ASC-SF induced increases in microfibril protein fibrillin-1, organizational matricellular protein fibulin-5, and cross-linking proteins lysyl oxidase (LOX) and lysyl oxidase-like 1 (LOXL-1). Fibulin-4 expression was unchanged with both ASC-SF stimulation and NCM when compared to NT, and LTBP-4 expression was significantly reduced with both ASC-SF stimulation and NCM.

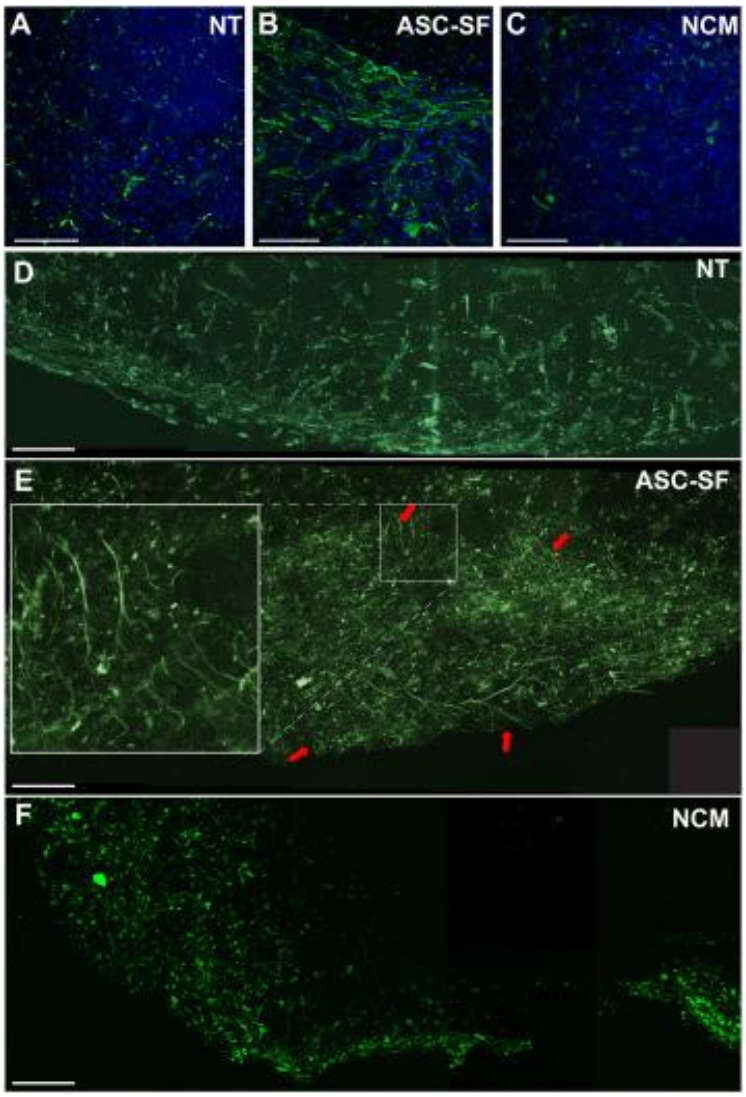

Figure 3: Induction of elastic fiber deposition by ASC-SF, as revealed by immunofluorescence and multiphoton microscopy. SMC elastic fibers (green) were revealed after ASC-SF stimulation (B), when compared to both No Treatment (A, NT) and Non-Conditioned Media (C, NCM) negative controls, in sample images of z-stacked confocal images of 30-day discs. Note that cellularity (nuclear stain, blue) is similar among groups. Separate discs were then analyzed by multiphoton microscopy using a Zeiss Plan-Apochromat 20× objective. (D) Composite image (1 × 5) of a representative NT control disc. (E) Composite image (2 × 5) of a representative ASC-SF stimulated disc. Arrows indicate areas of elastic fiber autofluorescence, and inset illustrates detail of elastic fibers. (F) Composite image (2 × 5) of a representative NCM-stimulated disc. All scale bars = 100 μm.

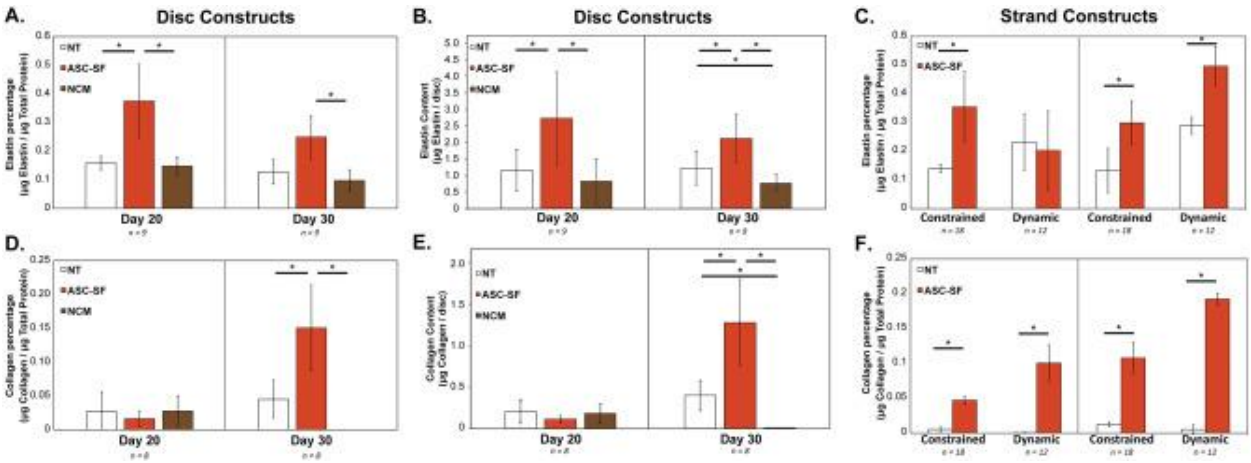

Figure 4: Insoluble elastin and collagen are enhanced by ASC-SF stimulation of SMCs, under varying geometries and loading conditions. (A–D) Discs were analyzed for (A) insoluble elastin percentage of total protein, (B) insoluble elastin per disc, (C) collagen percentage of total protein, and (D) collagen per disc, comparing control NT and NCM treatments with ASC-SF stimulation. (C, F) Strands were analyzed for (C) insoluble elastin percentage and (F) collagen percentage of total protein, comparing NT control treatment to ASC-SF stimulation under constrained and dynamic loading conditions.

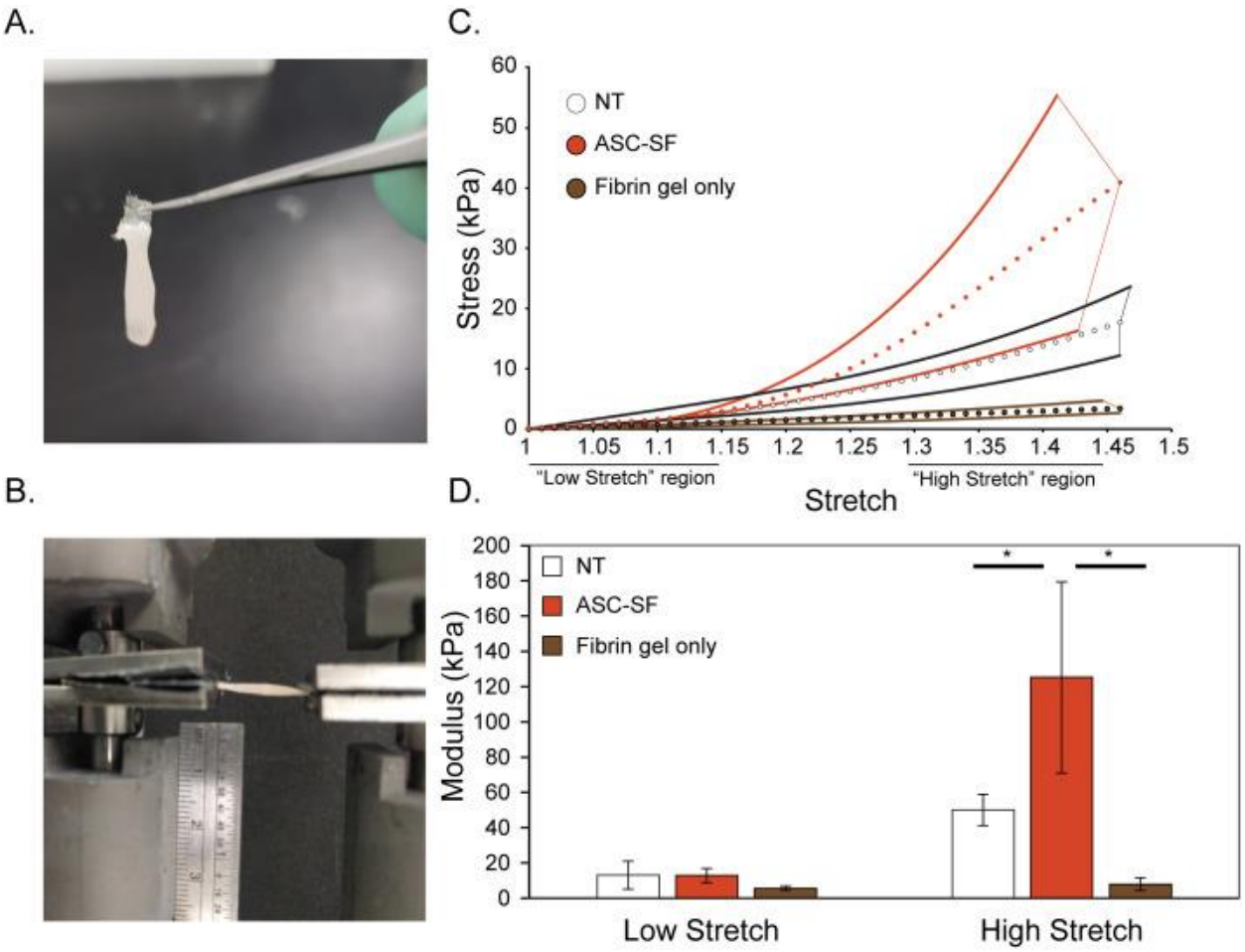

Figure 5: Shift in strand mechanical properties after ASC-SF stimulation. (A) Photo of fibrin removed from top half of nylon tabs of TissueTrain plates, resulting in an exposed tab that can be dried and clamped by sandpaper-aided pneumatic clamps. (B) Image of tensile testing configuration (Instron #5543A, with sandpaper-lined pneumatic clamps) used to test 30-day NT and ASC-SF treated strands, with ruler for scale. (C) For each sample group, the range of maximum and minimum stress values was plotted as a pair of thick lines, with the average values plotted as small circles. “Low” and “High” stretch regions are indicated, for each sample this was the first and final 1/3 of data points, respectively. (D) Comparison of low and high stretch elastic modulus for both 30-day NT and ASC-SF stimulated strands, alongside cell-free fibrin gel constructs.

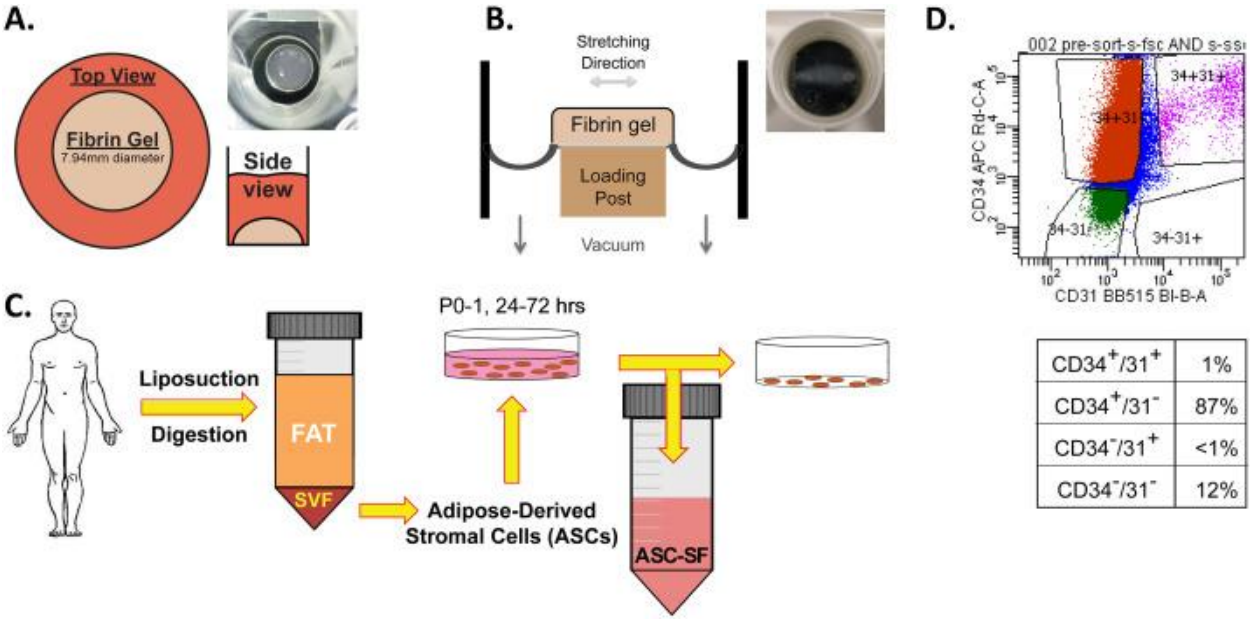

$CD34^{+}/31^{+}$	1%
$CD34^{+}/31^{-}$	87%
$CD34^{-}/31^{+}$	<1%
$CD34^{-}/31^{-}$	12%

Figure 6: Three-dimensional fibrin gel culture constructs and ASC-SF collection. (A) Fibrin gel “discs” (200 µL), plated on 24-well tissue culture plates within 7.94 mm diameter heat-stamped templates. (B) Fibrin gel “strands” (600 µL), plated between nylon tabs of FlexCell Linear TissueTrain untreated plates. Note that the discs are cultured on top of stiff tissue culture plastic while strands are cultured on top of a flexible silicone membrane. In the schematic, the long dimension is shown to illustrate the direction of constraint and dynamic stretch, however the overall geometry differs from a disc (see top view in photo). (C) ASC isolation following body-sculpting surgeries of non-smoking, non-diabetic patients below 45 years old. Stromal vascular fraction (SVF) is obtained following adipose tissue mincing and collagenase digestion, and ASCs are cultured within standard tissue culture flasks. Conditioned media (ASC-CM) is collected every 24–72 h in culture, from passages 0 to 1. (D) ASCs were sorted by flow cytometry according to staining for CD31 and CD34 cell markers, and then quantified according to percent in each subpopulation. Note the predominance of CD34+/CD31− cells (87%) among the ASCs used for media conditioning.